Hindawi
International Journal of Aerospace Engineering
Volume 2022, Article ID 4253558, 9 pages
https://doi.org/10.1155/2022/4253558

Research Article

Artificial Potential Field-Based Multi-UAV Formation Control and Target Tracking

He Song[1], **Shaolin Hu**[1,2], **Wenqiang Jiang**[1], **Qiliang Guo**[1], **and Ming Zhu**[3]

[1]*School of Automation and Information Engineering, Xi'an University of Technology, Xi'an, Shaanxi 710048, China*
[2]*School of Automation, Guangdong University of Petrochemical Technology, Maoming, Guangdong 525000, China*
[3]*Wuxi Kunlun Fuji Instruments Co., Ltd., Wuxi, Jiangxi 215200, China*

Correspondence should be addressed to Shaolin Hu; hfkth@126.com

Received 30 March 2022; Accepted 22 July 2022; Published 9 August 2022

Academic Editor: Xingling Shao

To simultaneously achieve space formation flight and target tracking of multiple unmanned aerial vehicles (UAVs) and solve the rotation buffeting problem of the UAV, a robust formation control and target tracking algorithm is proposed. The artificial potential function consisting of formation control term and target tracking term is established, and its convergence is proved. The sliding mode control method with the saturation function is established, and a sufficient condition for sliding mode to occur is analysed. Finally, the numerical simulation is conducted for the proposed algorithm, and the simulation result is analysed. The results show that the proposed algorithm can quickly achieve the formation flight and target tracking of multi-UAVs and improve the tracking performance; meanwhile, it can effectively weaken the rotation buffeting and improve the robustness.

1. Introduction

In recent years, along with the improvement and development of sensor technology and wireless communication technology and intelligent control technology, the UAV has been widely used in military and civilian fields and has achieved remarkable results [1, 2]. Compared with a single UAV system, a multi-UAV system can effectively overcome the shortcomings of the single UAV system and improve the overall performance of the system under the reasonable utilization of resources. It also has obvious advantages in performing complex and diverse tasks such as formation flight, dynamic target tracking, and interception and has gradually become a research hotspot [3–6].

At present, aiming to the problem of the formation control and target tracking of a multi-UAV system, experts and scholars have done many works and obtained a lot of research results. For the formation control, the commonly employed approaches include leader-following methods [7, 8], virtual structure methods [9], behavior-based control methods [10], graph theory methods [11, 12], model predictive control methods [13], and consistency theory methods [14]. However, these approaches usually need to establish accurate mathematical models, which severely limit their scope of application. Recently, along with the rise of machine learning algorithms, the outstanding advantages of machine learning have attracted the attention of more and more researchers, who have begun to use them to solve the problems of the coordinated control of formation flight in multi-UAV systems. An aggregation strategy based on the *Q*-learning algorithm and potential field approach was proposed to achieve the coordinated control of multi-UAVs [15]; a control framework of multiagent self-organizing aggregation behavior based on *Q*-learning algorithm was designed in reference [16], and simulation experiments show that multiagents can not only complete self-organizing aggregation tasks but also exhibit antipredation behavior and avoid predators; a hybrid system based on reinforcement learning and aggregation control was proposed in [17, 18], and the simulation and experiments illustrate the stability and effectiveness of the hybrid system; a coordination control method of UAV formation flight based on the DDPG algorithm is proposed in

[19], which enables the UAV to complete the aggregation task in complex and diverse environments. For the target tracking, considering the change of the tracking distance, based on the Lyapunov navigation vector field, a coordinated tracking method was proposed to realize the tracking of moving target groups by multiple UAVs [20]; in order to satisfy the requirements of obstacle avoidance, a method based on the Lyapunov navigation vector field and artificial potential field was proposed to complete target tracking task [21]; a dynamic path planning algorithm based on the tangent vector navigation vector field and the Lyapunov navigation vector field was proposed for the quadrotor to track the ground target [22]; aiming to the influence of target speed, a modified Lyapunov navigation vector field method was proposed to complete the tracking of ground moving targets [23]; a guidance method based on the Lyapunov vector field was proposed to solve the problem of coordinated tracking of multiple UAVs [24]; the reference point guidance was modified to the lateral guidance law of the quadrotor, and the mathematical model of the relative distance between the quadrotor and the target was established by nonlinear differential equations; finally, a Lyapunov navigation vector field method including the curvature-constrained was proposed to complete the target tracking task [25]. However, the above mentioned methods usually have separated formation control and target tracking and separately studied the formation control or target tracking of multi-UAVs. Yao et al. realized the target tracking and formation control of the intelligent cluster based on the potential function and the sliding mode control method [26]. However, due to the use of symbolic functions to design the motion control rate of the intelligent body, the chattering of the intelligent cluster was relatively large, which affected the tracking and control accuracy of the intelligent cluster.

Based on the above research results and existing problems, the flight control rate based on the saturation function is designed, and an improved artificial potential function combined with sliding mode control is proposed to realize the target tracking and formation control of multiple UAVs. The paper is organized as follows: in Section 2, an artificial potential function including formation control items and target tracking items is constructed, and its convergence is proved, and the sliding mode control method based on the saturation function is established to weaken the rotation buffeting of the UAV; in Section 3, numerical simulation method is used to analyse and verify the effectiveness of the proposed algorithm; finally, conclusions are made in Section 4.

2. Formation Control and Target Tracking Method Based on Improved Potential Function Model and Sliding Mode Control

2.1. Artificial Potential Function Model. The artificial potential function is a virtual potential field function and is proposed by Khatib in 1994 [26], in the virtual potential field, the agent receives the gravitational force of the target point and the repulsion force of the obstacle at the same time, and the agent moves under the action of the resultant force. The form of the potential function is not unique. It can be designed according to the structure or behavior of the group and is being used in the field of aggregation intelligence, formation control, and multiagent coordination [27, 28, 29].

Considering a multiagent system consisting of N UAVs, the artificial potential function is established to realize the mission of target tracking and formation control. For the convenience of description, define the Nth UAV as the target UAV, and the other $N-1$ UAVs as the tracking UAV, and the position vector of the target UAV and the tracking UAV relative to the ground coordinate system as $\vec{x}_N$ and $\vec{x}_i$ $(i = 1, 2, \cdots, N-1)$, respectively. The kinematic model of all UAVs is the same and can be expressed as [30]

$$\begin{cases} \dot{x}_{i1} = v_i \cos \chi_i \cos \delta_i, \\ \dot{x}_{i2} = v_i \sin \chi_i \cos \delta_i, \\ \dot{x}_{i3} = v_i \sin \delta_i, \end{cases} \tag{1}$$

where $\vec{x}_i = [x_{i1}\ x_{i2}\ x_{i3}]^T$ is the position vector of the ith UAV, v_i is the flight velocity of the ith UAV, and χ_i and δ_i are the yaw angle and pitch angle of the ith UAV.

In this paper, our objective is to make the tracking UAV gradually approach the target UAV and eventually aggregate around the target UAV in a form of formation flight. In fact, this is a solution to the problem of coordinated control tracking of multi-UAVs.

In order to ensure that the tracking UAV can track the target UAV and realize formation control, the following potential function is used [26].

$$J\left(\vec{x}, \vec{x}_N\right) = k_N \sum_{i=1}^{N-1} J_{\mathrm{iN}}\left(\left\|\vec{x}_i - \vec{x}_N\right\|\right) + k_f \sum_{i=1}^{N-2} \sum_{j=i+1}^{N-1} J_{ij}\left(\left\|\vec{x}_i - \vec{x}_j\right\|\right), \tag{2}$$

where k_N and k_f are weight coefficients, the potential function $J_{\mathrm{iN}}(\|\vec{x}_i - \vec{x}_N\|)$ is the function of the distance $\|\vec{x}_i - \vec{x}_N\|$ between the tracking and the target, and the potential function $J_{ij}(\|\vec{x}_i - \vec{x}_j\|)$ is the function of the distance $\|\vec{x}_i - \vec{x}_j\|$ between tracking UAVs.

Considering the distance margin, the tracking UAV tracks the target UAV at a certain distance c_1, and the following conditions must be met:

$$\lim_{t \longrightarrow \infty} J_{\mathrm{iN}}\left(\left\|\vec{x}_i - \vec{x}_N\right\|\right) = c_1. \tag{3}$$

Similarly, the tracking aircraft and the tracking aircraft form a formation flying at a certain distance c_2, and the following conditions must be met:

$$\lim_{t \longrightarrow \infty} J_{ij}\left(\left\|\vec{x}_i - \vec{x}_j\right\|\right) = c_2. \tag{4}$$

Multiple UAVs can achieve target tracking and formation control, and the following conditions must be met:

$$\lim_{t\longrightarrow\infty} J\left(\vec{x}, \vec{x}_N\right) = c. \tag{5}$$

According to the result of Equation (5), the potential function $J(\vec{x}, \vec{x}_N)$ converges.

Introducing the definition of potential function [26], we can know that it is a differentiable, nonnegative, and decreasing function, and its time derivative can be got:

$$\dot{J} = \sum_{i=1}^{N-1} \left[\nabla_{\vec{x}_i} J\left(\vec{x}, \vec{x}_N\right)\right]^T \dot{\vec{x}}_i + \left[\nabla_{\vec{x}_N} J\left(\vec{x}, \vec{x}_N\right)\right]^T \dot{\vec{x}}_N. \tag{6}$$

Actually, in most circumstances, the current velocities of the tracking and the target are unknown and difficult to assume in advance. In this regard, the following assumptions are made:

(1) The flight velocity of the target meets $\|\dot{\vec{x}}_N\| \le \nu_N$ for any known the velocity variable $\nu_N > 0$

(2) The relative position of the target and the tracking is known, and the relative positions of the tracking UAVs are known

Based on the above assumptions, without considering the size and dimension of the UAV, the flight control law of the tracking UAV can be designed as [26]:

$$\dot{\vec{x}}_i = \vec{u}_i = -\alpha \nabla_{\vec{x}_i} J\left(\vec{x}, \vec{x}_N\right) - \beta \text{sat}\left(\nabla_{\vec{x}_i} J\left(\vec{x}, \vec{x}_N\right), \gamma\right), \tag{7}$$

where $\vec{u}_i$ is the control input, α and β are positive constants, $\beta \ge \nu_N$, sat$(\cdot)$ is a saturation function, γ is the function boundary thickness, and the saturation function can be given by

$$\text{sat}\left(\nabla_{\vec{x}_i} J\left(\vec{x}, \vec{x}_N\right), \gamma\right) = \begin{cases} \text{sign}\left(\nabla_{\vec{x}_i} J\left(\vec{x}, \vec{x}_N\right)\right), & \left\|\nabla_{\vec{x}_i} J\left(\vec{x}, \vec{x}_N\right)\right\| \ge \|\gamma\|, \\ \dfrac{\nabla_{\vec{x}_i} J\left(\vec{x}, \vec{x}_N\right)}{\gamma}, & \left\|\nabla_{\vec{x}_i} J\left(\vec{x}, \vec{x}_N\right)\right\| < \|\gamma\|. \end{cases} \tag{8}$$

After combining Equations (6) and (7), we can obtain:

$$\begin{aligned} \dot{J} = & \sum_{i=1}^{N-1} \left[\nabla_{\vec{x}_i} J\left(\vec{x}, \vec{x}_N\right)\right]^T \\ & \cdot \left[-\alpha \nabla_{\vec{x}_i} J\left(\vec{x}, \vec{x}_N\right) - \beta \text{sat}\left(\nabla_{\vec{x}_i} J\left(\vec{x}, \vec{x}_N\right), \gamma\right)\right] \\ & + \left[\nabla_{\vec{x}_N} J\left(\vec{x}, \vec{x}_N\right)\right]^T \dot{\vec{x}}_N. \end{aligned} \tag{9}$$

Case 1. When $\|\nabla_{\vec{x}_i} J(\vec{x}, \vec{x}_N)\| \ge \|\gamma\|$, Equation (9) can be written as:

$$\begin{aligned} \dot{J} = & \sum_{i=1}^{N-1} \left[\nabla_{\vec{x}_i} J\left(\vec{x}, \vec{x}_N\right)\right]^T \\ & \cdot \left[-\alpha \nabla_{\vec{x}_i} J\left(\vec{x}, \vec{x}_N\right) - \beta \text{sign}\left(\nabla_{\vec{x}_i} J\left(\vec{x}, \vec{x}_N\right)\right)\right] \\ & + \left[\nabla_{\vec{x}_N} J\left(\vec{x}, \vec{x}_N\right)\right]^T \dot{\vec{x}}_N \le -\alpha \sum_{i=1}^{N-1} \left\|\nabla_{\vec{x}_i} J\left(\vec{x}, \vec{x}_N\right)\right\|^2 \\ & - \beta \sum_{i=1}^{N-1} \left\|\nabla_{\vec{x}_i} J\left(\vec{x}, \vec{x}_N\right)\right\| + \nu_N \sum_{i=1}^{N-1} \left\|\nabla_{\vec{x}_i} J\left(\vec{x}, \vec{x}_N\right)\right\|. \end{aligned} \tag{10}$$

Owing to $\beta \ge \nu_N$, we can get:

$$\dot{J} \le -\alpha \sum_{i=1}^{N-1} \left\|\nabla_{\vec{x}_i} J\left(\vec{x}, \vec{x}_N\right)\right\|^2. \tag{11}$$

According to the LaSalle Yoshizawa theory [31], we can obtain:

$$\lim_{t\longrightarrow\infty} \sum_{i=1}^{N-1} \left\|\nabla_{\vec{x}_i} J\left(\vec{x}, \vec{x}_N\right)\right\|^2 = 0. \tag{12}$$

Therefore,

$$\lim_{t\longrightarrow\infty} \dot{J} = 0 \, J\left(\vec{x}, \vec{x}_N\right). \tag{13}$$

Equation (13) shows that as time tends to infinity, the potential function converges.

Case 2. When $\|\nabla_{\vec{x}_i} J(\vec{x}, \vec{x}_N)\| < \|\gamma\|$, Equation (9) can be written as:

$$\begin{aligned} \dot{J} = & \sum_{i=1}^{N-1} \left[\nabla_{\vec{x}_i} J\left(\vec{x}, \vec{x}_N\right)\right]^T \left[-\alpha \nabla_{\vec{x}_i} J\left(\vec{x}, \vec{x}_N\right) - \beta \frac{\nabla_{\vec{x}_i} J\left(\vec{x}, \vec{x}_N\right)}{\gamma}\right] \\ & + \left[\nabla_{\vec{x}_N} J\left(\vec{x}, \vec{x}_N\right)\right]^T \dot{\vec{x}}_N \le -\alpha \sum_{i=1}^{N-1} \left\|\nabla_{\vec{x}_i} J\left(\vec{x}, \vec{x}_N\right)\right\|^2 \\ & - \frac{\beta}{\gamma} \sum_{i=1}^{N-1} \left\|\nabla_{\vec{x}_i} J\left(\vec{x}, \vec{x}_N\right)\right\|^2 + \nu_N \sum_{i=1}^{N-1} \left\|\nabla_{\vec{x}_i} J\left(\vec{x}, \vec{x}_N\right)\right\| \\ \le & -\left(\alpha + \frac{\beta}{\gamma}\right) \sum_{i=1}^{N-1} \left\|\nabla_{\vec{x}_i} J\left(\vec{x}, \vec{x}_N\right)\right\|^2 + \nu_N \sum_{i=1}^{N-1} \left\|\nabla_{\vec{x}_i} J\left(\vec{x}, \vec{x}_N\right)\right\|. \end{aligned} \tag{14}$$

According to Equation (12), we can get:

$$\lim_{t\longrightarrow\infty} \left\|\nabla_{\vec{x}_i} J\left(\vec{x}, \vec{x}_N\right)\right\| = 0. \tag{15}$$

After combining Equations (12), (14), and (15), we can obtain:

$$\lim_{t\longrightarrow\infty} \dot{J} = 0. \tag{16}$$

Similarly, it is proved that as time tends to infinity, the potential function $J(\vec{x}, \vec{x}_N)$ converges.

Combining Equation (6), we can get:

$$\lim_{t\longrightarrow\infty}\left\|\nabla_{\vec{x}_N} J\left(\vec{x}, \vec{x}_N\right)\right\| = 0, \tag{17}$$

$$\lim_{t\longrightarrow\infty}\left(\vec{x}, \vec{x}_N\right) \longrightarrow \Omega, \tag{18}$$

where $\Omega = \{(\vec{x}, \vec{x}_N) | \nabla_{\vec{x}_N} J(\vec{x}, \vec{x}_N) = 0, \nabla_{\vec{x}_i} J(\vec{x}, \vec{x}_N) = 0, i = 1, 2, \cdots, N-1\}$.

Equation (18) also proves that as time tends to infinity, the potential function $J(\vec{x}, \vec{x}_N)$ converges. Therefore, Equation (5) can be satisfied, and the tracking UAV can not only complete the task of tracking the target UAV but also realize formation flight control.

The above results regard the UAV as a mass point, which reflect the behavioural process of target tracking and formation control and give a proof of the concept. However, it does not consider the dynamic control of the UAV. In the next section, we will discuss a control algorithm based on sliding mode control theory which can make the UAV achieve the desired motion.

2.2. Sliding Model Control. In the preceding section, using the flight control rate as shown in Equation (7), the particle target tracking and formation control are realized. In this section, considering the complex dynamics model of the tracking, a sliding mode control method based on the saturation function is established to realize the desired motion of the tracking. The kinematic model of the tracking UAV can be described as [32]

$$M\left(\vec{x}_i\right)\ddot{\vec{x}}_i + f_i\left(\vec{x}_i, \dot{\vec{x}}_i\right) = \vec{u}_i, \tag{19}$$

where $M(\vec{x}_i)$ is the mass or inertia matrix and $f_i(\vec{x}_i, \dot{\vec{x}}_i)$ is function including disturbances and other effects and is defined as

$$f_i\left(\vec{x}_i, \dot{\vec{x}}_i\right) = f_i^{\text{known}}\left(\vec{x}_i, \dot{\vec{x}}_i\right) + f_i^{\text{unknown}}\left(\vec{x}_i, \dot{\vec{x}}_i\right), \tag{20}$$

where $f_i^{\text{known}}(\vec{x}_i, \dot{\vec{x}}_i)$ is the known disturbances and $f_i^{\text{unknown}}(\vec{x}_i, \dot{\vec{x}}_i)$ is the unknown effects.

Assuming that $\|f_i^{\text{unknown}}(\vec{x}_i, \dot{\vec{x}}_i)\| \le \bar{f}_i$, $\bar{f}_i < \infty$ is a known constant. In addition, we also assume that the matrix $M(\vec{x}_i)$ satisfies the following conditions for all $\vec{x}_i$:

$$\underline{M}\left\|\vec{y}\right\|^2 \le \vec{y}^T M\left(\vec{x}_i\right)\vec{y} \le \bar{M}\left\|\vec{y}\right\|^2, \tag{21}$$

where M and $-M$ are known constant and $\vec{y}$ is an arbitrary vector.

Given the above kinematic model, we will choose the control input $\vec{u}_i$ using the sliding mode control method to make the flight velocity of UAVs meet the requirement of Equation (7). The sliding manifold can be chosen:

$$\vec{s}_i = \dot{\vec{x}}_i + \alpha\nabla_{\vec{x}_i} J\left(\vec{x}, \vec{x}_N\right) + \beta\text{sat}\left(\nabla_{\vec{x}_i} J\left(\vec{x}, \vec{x}_N\right), \gamma\right). \tag{22}$$

Based on the sliding mode control theory [32], the sufficient condition for the tracker to reach the sliding manifold is

$$\vec{s}_i^T \dot{\vec{s}}_i < 0. \tag{23}$$

Therefore, in order to ensure the sliding manifold can be asymptotically reached in a finite time, a control input $\vec{u}_i$ can be designed as

$$\vec{u}_i = -u_0 \text{ sign}\left(\vec{s}_i\right) + f_i^{\text{known}}\left(\vec{x}, \dot{\vec{x}}_i\right). \tag{24}$$

According to the characteristics of the saturation function sat$(\cdot)$, the choice of the control gain u_0 can be discussed in the following two cases.

Case 1. When $\|\nabla_{\vec{x}_i} J(\vec{x}, \vec{x}_N)\| \ge \|\gamma\|$, Equations (22) can be rewritten as:

$$\vec{s}_i = \dot{\vec{x}}_i + \alpha\nabla_{\vec{x}_i} J\left(\vec{x}, \vec{x}_N\right) + \beta \text{ sign}\left(\nabla_{\vec{x}_i} J\left(\vec{x}, \vec{x}_N\right)\right). \tag{25}$$

From Equation (25), the term β sign $(\nabla_{\vec{x}_i} J(\vec{x}, \vec{x}_N))$ is not differentiable, in order to solve this problem, drawing on the idea of the equivalent control method and sliding mode observers, a first-order low pass filter can be defined as [32, 33].

$$\lambda\dot{z} + z = \beta \text{ sign}\left(\nabla_{\vec{x}_i} J\left(\vec{x}, \vec{x}_N\right)\right), \tag{26}$$

where λ is a small positive constant, the β sign $(\nabla_{\vec{x}_i} J(\vec{x}, \vec{x}_N))$ is the input, and z is the filtered output.

The term β sign $(\nabla_{\vec{x}_i} J(\vec{x}, \vec{x}_N))$ has an equivalent component and a high frequency component during sliding mode. The low pass filter can cut the high frequency component. The equivalent component is denoted as $[\beta \text{ sign } (\nabla_{\vec{x}_i} J(\vec{x}, \vec{x}_N))]_{\text{eq}}$, with the proper value of the parameters λ, we can get

$$z \approx \left[\beta \text{ sign}\left(\nabla_{\vec{x}_i} J\left(\vec{x}, \vec{x}_N\right)\right)\right]_{\text{eq}}. \tag{27}$$

Using z to replace $[\beta \text{ sign } (\nabla_{\vec{x}_i} J(\vec{x}, \vec{x}_N))]$ in Equation (25), we can get

$$\vec{s}_i = \dot{\vec{x}}_i + \alpha\nabla_{\vec{x}_i} J\left(\vec{x}, \vec{x}_N\right) + z. \tag{28}$$

Now, we will determine the choice of the control gain u_0.

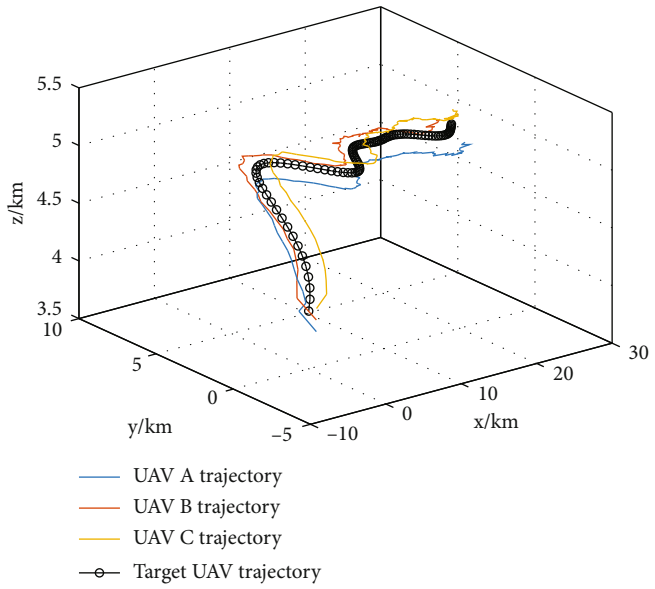

Figure 1: The tracking trajectories of the traditional algorithm.

Theorem 1. *Based on Equations (24)~(30), the sufficient condition* $\vec{s}_i^T \dot{\vec{s}}_i < 0$ *is satisfied; the control gain* u_0 *should meet the following condition:*

$$u_0 > \bar{M}\left(-\frac{1}{\underline{M}}\bar{f}_i + \bar{J} + \bar{J}_{\text{sign}} + \varepsilon\right), \tag{29}$$

where ε *is a small positive constant.*

Proof. The time derivative of Equation (28) is

$$\dot{\vec{s}}_i = \ddot{\vec{x}}_i + \frac{d}{dt}\left[\alpha\nabla_{\vec{x}_i} J\left(\vec{x}, \vec{x}_N\right)\right] + \dot{z}. \tag{30}$$

□

Case 2. When $\|\nabla_{\vec{x}_i} J(\vec{x}, \vec{x}_N)\| < \|\gamma\|$, Equation (22) can be rewritten as:

$$\vec{s}_i = \dot{\vec{x}}_i + \alpha\nabla_{\vec{x}_i} J\left(\vec{x}, \vec{x}_N\right) + \frac{\beta}{\gamma}\nabla_{\vec{x}_i} J\left(\vec{x}, \vec{x}_N\right). \tag{31}$$

According to the results of Equations (19) and (24), we can get

$$\begin{aligned}\vec{s}_i^T \dot{\vec{s}}_i = -\vec{s}_i^T \Big[&M^{-1}\left(\vec{x}_i\right) u_0 \text{ sign } \left(\vec{s}_i\right) \\ &+ M^{-1}\left(\vec{x}_i\right) f_i^{\text{unknown}}\left(\vec{x}_i, \dot{\vec{x}}_i\right) \\ &- \frac{d}{dt}\left[\alpha\nabla_{\vec{x}_i} J\left(\vec{x}, \vec{x}_N\right)\right] - \dot{z}\Big].\end{aligned} \tag{32}$$

For the right hand side of Equation (32), we can get

$$\begin{aligned}&\left\|\vec{s}_i^T\left[M^{-1}\left(\vec{x}_i\right) u_0 \text{ sign } \left(\vec{s}_i\right) + M^{-1}\left(\vec{x}_i\right) f_i^{\text{unknown}}\left(\vec{x}_i, \dot{\vec{x}}_i\right) - \frac{d}{dt}\left[\alpha\nabla_{\vec{x}_i} J\left(\vec{x}, \vec{x}_N\right)\right] - \dot{z}\right]\right\| \le \\ &\left\|\vec{s}_i\right\|\left\|M^{-1}\left(\vec{x}_i\right) u_0 \text{ sign } \left(\vec{s}_i\right) + M^{-1}\left(\vec{x}_i\right) f_i^{\text{unknown}}\left(\vec{x}_i, \dot{\vec{x}}_i\right) - \frac{d}{dt}\left[\alpha\nabla_{\vec{x}_i} J\left(\vec{x}, \vec{x}_N\right)\right] - \dot{z}\right\| \le \\ &\left\|\vec{s}_i\right\|\left[\left\|M^{-1}\left(\vec{x}_i\right) u_0 \text{ sign } \left(\vec{s}_i\right)\right\| + \left\|M^{-1}\left(\vec{x}_i\right) f_i^{\text{unknown}}\left(\vec{x}_i, \dot{\vec{x}}_i\right)\right\| - \left\|\frac{d}{dt}\left[\alpha\nabla_{\vec{x}_i} J\left(\vec{x}, \vec{x}_N\right)\right]\right\| - \|\dot{z}\|\right].\end{aligned} \tag{33}$$

According to the result of Equation (15), we can get

$$\left\|\frac{d}{dt}\left[\alpha\nabla_{\vec{x}_i} J\left(\vec{x}, \vec{x}_N\right)\right]\right\| \le \bar{J}, \tag{34}$$

where $\bar{J}$ is a known constant, and its value range is $0 < \bar{J} < \infty$.

And according to the results of Equations (26) and (27), we can get

$$\|\dot{z}\| = \left\|\frac{1}{\lambda}\left[-z + \beta \text{ sign } \left(\nabla_{\vec{x}_i} J\left(\vec{x}, \vec{x}_N\right)\right)\right]\right\| \le \frac{2\beta}{\lambda} \triangleq \bar{J}_{\text{sign}}, \tag{35}$$

where $\bar{J}_{\text{sign}}$ is a known constant, and its value range is $0 < \bar{J}_{\text{sign}} < \infty$.

Based on the results of Equations (21), (24), (34), and (35), we can get

$$\vec{s}_i^T \dot{\vec{s}}_i < -\left\|\vec{s}_i\right\|\left[\frac{1}{\bar{M}} u_0 + \frac{1}{\underline{M}}\bar{f}_i - \bar{J}_{\text{sign}} - \bar{J}\right]. \tag{36}$$

If satisfying the sufficient condition $\vec{s}_i^T \dot{\vec{s}}_i < 0$, we can obtain

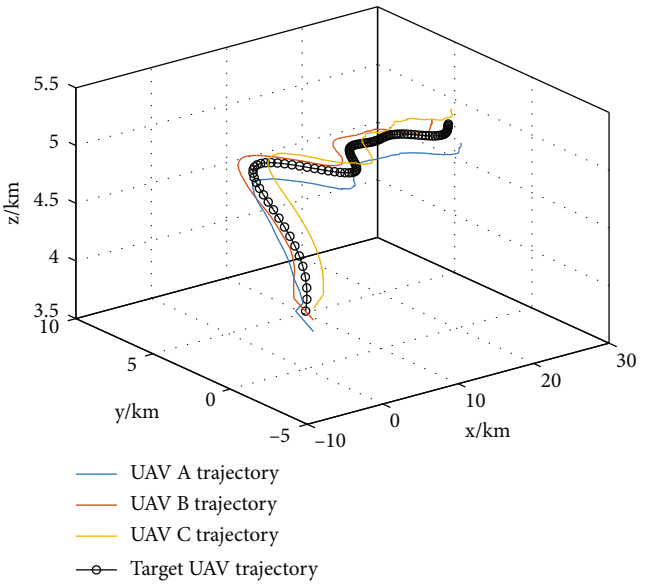

Figure 2: The tracking trajectories of proposed algorithm.

$$u_0 > \bar{M}\left(-\frac{1}{\underline{M}}\bar{f}_i + \bar{J}_{\text{sign}} + \bar{J} + \varepsilon\right). \tag{37}$$

For any $\varepsilon > 0$, $\vec{s}_i^T \dot{\vec{s}}_i < -\varepsilon\|\vec{s}_i\|$ is satisfied; in other words, once the tracking reaches the sliding manifold ($\vec{s}_i = 0$) asymptotically in a finite tome, it will remain on that manifold for all time.

This proof is completed.

The time derivative of Equation (31) is

$$\begin{aligned}\dot{\vec{s}}_i &= \ddot{\vec{x}}_i + \frac{d}{dt}\left[\alpha\nabla_{\vec{x}_i}J\left(\vec{x}, \vec{x}_N\right)\right] + \frac{d}{dt}\left[\frac{\beta}{\gamma}\nabla_{\vec{x}_i}J\left(\vec{x}, \vec{x}_N\right)\right] \\ &= \ddot{\vec{x}}_i + \frac{d}{dt}\left[\left(\alpha + \frac{\beta}{\gamma}\right)\nabla_{\vec{x}_i}J\left(\vec{x}, \vec{x}_N\right)\right].\end{aligned} \tag{38}$$

According to the results of Equations (19) and (24), we can get

$$\begin{aligned}\vec{s}_i^T\dot{\vec{s}}_i = -\vec{s}_i^T\Big[&M^{-1}\left(\vec{x}_i\right)u_0\ \text{sign}\left(\vec{s}_i\right) \\ &+ M^{-1}\left(\vec{x}_i\right)f_i^{\text{unknown}}\left(\vec{x}_i, \dot{\vec{x}}_i\right) \\ &- \frac{d}{dt}\left[\left(\alpha + \frac{\beta}{\gamma}\right)\nabla_{\vec{x}_i}J\left(\vec{x}, \vec{x}_N\right)\right]\Big].\end{aligned} \tag{39}$$

Due to

$$\begin{aligned}&\left\|\vec{s}_i^T\left[M^{-1}\left(\vec{x}_i\right)u_0\ \text{sign}\left(\vec{s}_i\right) + M^{-1}\left(\vec{x}_i\right)f_i^{\text{unknown}}\left(\vec{x}_i, \dot{\vec{x}}_i\right) - \frac{d}{dt}\left[\left(\alpha + \frac{\beta}{\gamma}\right)\nabla_{\vec{x}_i}J\left(\vec{x}, \vec{x}_N\right)\right]\right]\right\| \le \\ &\left\|\vec{s}_i\right\|\left\|M^{-1}\left(\vec{x}_i\right)u_0\ \text{sign}\left(\vec{s}_i\right) + M^{-1}\left(\vec{x}_i\right)f_i^{\text{unknown}}\left(\vec{x}_i, \dot{\vec{x}}_i\right) - \frac{d}{dt}\left[\left(\alpha + \frac{\beta}{\gamma}\right)\nabla_{\vec{x}_i}J\left(\vec{x}, \vec{x}_N\right)\right]\right\| \le \\ &\left\|\vec{s}_i\right\|\left[\left\|M^{-1}\left(\vec{x}_i\right)u_0\ \text{sign}\left(\vec{s}_i\right)\right\| + \left\|M^{-1}\left(\vec{x}_i\right)f_i^{\text{unknown}}\left(\vec{x}_i, \dot{\vec{x}}_i\right)\right\| + \left\|\frac{d}{dt}\left[\left(\alpha + \frac{\beta}{\gamma}\right)\nabla_{\vec{x}_i}J\left(\vec{x}, \vec{x}_N\right)\right]\right\|\right],\end{aligned} \tag{40}$$

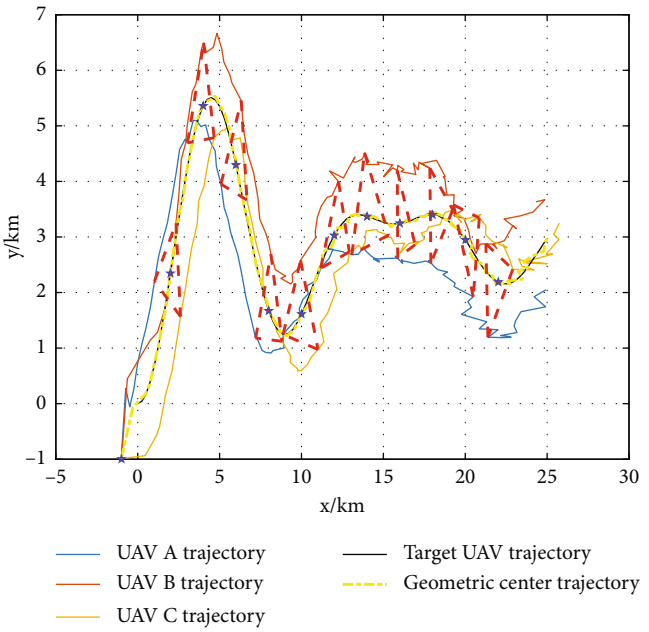

Figure 3: The X-Y coordinate change of the traditional algorithm.

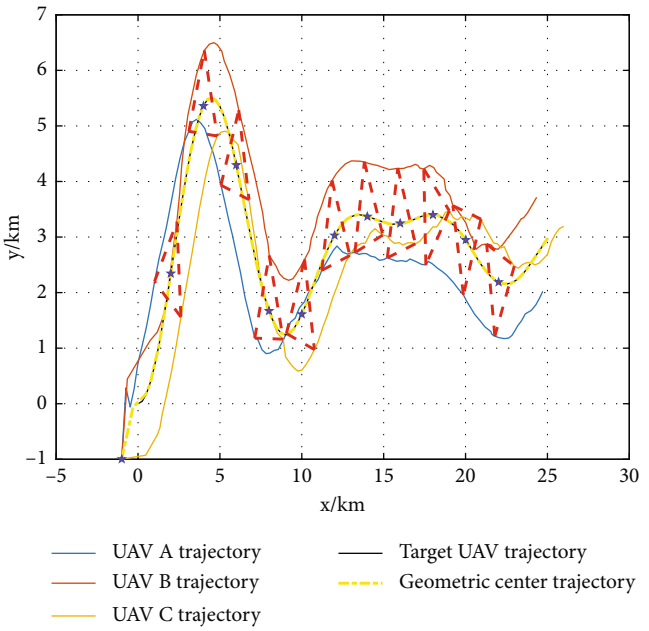

Figure 4: The X-Y coordinate change of proposed algorithm.

and according to the result of Equation (15), we can get

$$\left\|\frac{d}{dt}\left[\left(\alpha + \frac{\beta}{\gamma}\right)\nabla_{\vec{x}_i}J\left(\vec{x}, \vec{x}_N\right)\right]\right\| \le \bar{J}_s, \tag{41}$$

where $\bar{J}_s$ is a known constant, and its value range is $0 < \bar{J}_s < \infty$.

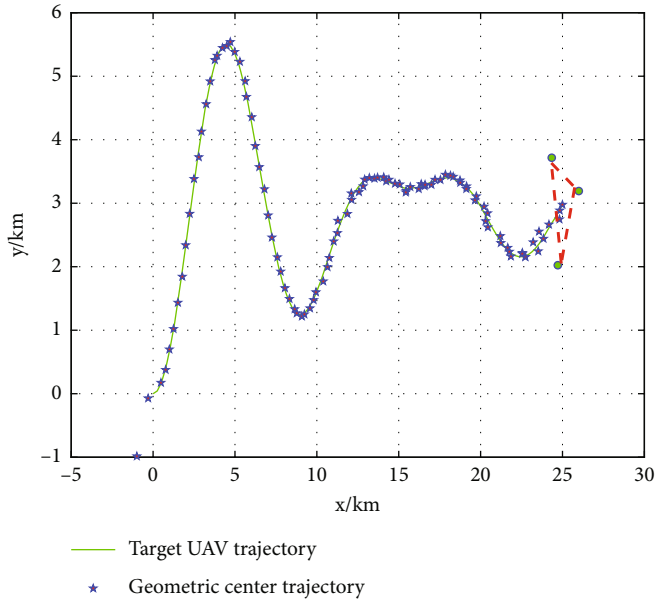

Figure 5: The geometric centre trajectory of traditional algorithm.

According to the results of Equations (21), (24), and (41), we can get

$$\vec{s}_i^T \dot{\vec{s}}_i < -\left\|\vec{s}_i\right\| \left[\frac{1}{\bar{M}} u_0 + \frac{1}{\underline{M}} \bar{f}_i - \bar{J}_s\right]. \tag{42}$$

If satisfying the sufficient condition $\vec{s}_i^T \dot{\vec{s}}_i < 0$, we can obtain

$$u_0 > \bar{M}\left(-\frac{1}{\underline{M}} \bar{f}_i + \bar{J}_s + \mu\right). \tag{43}$$

For any $\mu > 0$, $\vec{s}_i^T \dot{\vec{s}}_i < -\mu\|\vec{s}_i\|$ is satisfied; in other words, once the tracking reaches the sliding manifold ($\vec{s}_i = 0$) asymptotically in a finite tome, it will remain on that manifold for all time.

3. Numerical Simulations and Result Analysis

In this section, numerical simulation and result analysis of the proposed algorithm are carried out and compared with the traditional algorithm to illustrate the effectiveness and applicability of the proposed algorithm. Selecting the number of UAVs is $N = 4$, one of them is the target UAV, and the other three are used as tracking UAVs. Our objective is to achieve the formation flight of the three tracking UAV in a triangle while making the target in the midcentre of the triangle.

Assuming that the kinematic model of UAVs is the same, as shown in Equation (20) and set the relative parameter: the mass $M(\vec{x}_i) = 1$, $M = 0.5$, $-M = 1.5$, and $v_N = 10$. The unknown uncertainty $f_i(\vec{x}_i, \dot{\vec{x}}_i)$ can be replaced by random noise in this paper. The initial position of the target is [0, 0, 5] km, the initial position of tracking UAVs is randomly distributed near the origin and does not coincide with the position of the target.

The potential function is selected as

$$J\left(\vec{x}, \vec{x}_N\right) = \sum_{i=1}^{N-1} \frac{1}{2}\left(\left\|\vec{x}_i - \vec{x}_N\right\|^2\right) + \sum_{i=1}^{N-2}\sum_{j=i+1}^{N-1} \cdot \left[\frac{a}{2}\left\|\vec{x}_i - \vec{x}_j\right\|^2 + \frac{bc}{2}\left(-\frac{\left\|\vec{x}_i - \vec{x}_j\right\|^2}{c}\right)\right], \tag{44}$$

where $a = 1$, $b = 0.6$, and $c = 1.7$. The sliding mode controller parameters are $\alpha = 0.01$, $\beta = 2.0$, $\bar{f}_i = 1$, $\varepsilon = 1$, $u_0 = 125$, and $\mu = 0.1$, respectively.

All simulation parameter set are basically the same as those in [26]. The simulation results as follows.

From Figures 1 and 2, it can be seen that after a short period, the tracking UAV can catch with the target quickly and always gather near the target. Compared with the traditional algorithm, the proposed algorithm can reduce the rotation buffeting of the tracking UAV.

From Figures 3 and 4, it can be seen that after a short period, the three tracking UAV can gather near the target quickly in a triangular formation, and the midcentre trajectory of the triangle is very consistent with the flight trajectory of the target. Similarly, it can be also seen that the proposed algorithm can effectively reduce the rotation buffeting of the UAV.

From Figures 5 and 6, it can be seen that the tracking UAV can quickly form a triangular formation and gather near the target UAV and can always keep the triangle

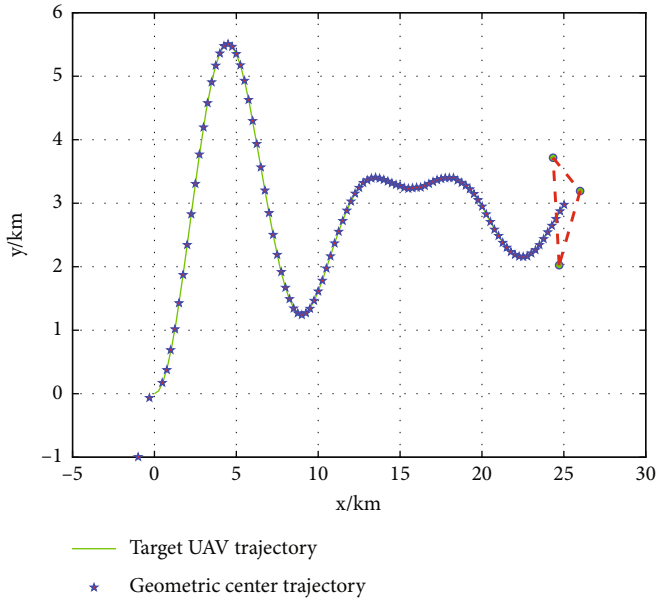

Figure 6: The geometric centre trajectory of the proposed algorithm.

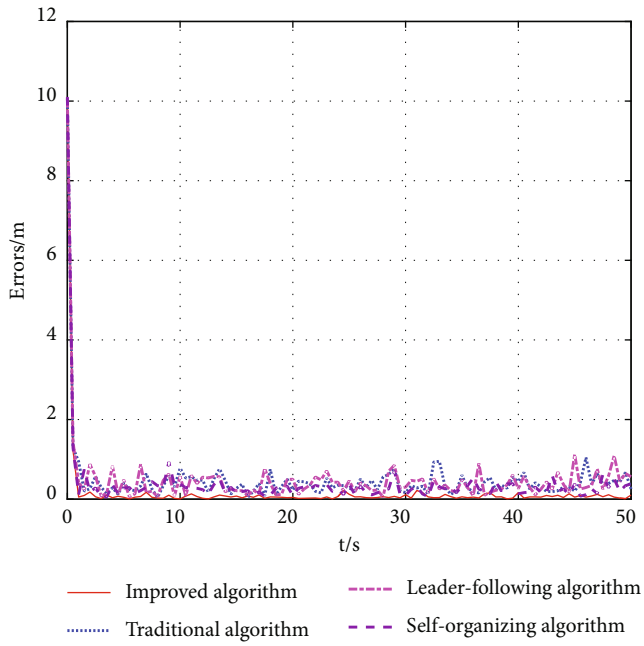

Figure 7: The error between the geometric centre trajectory and the target trajectory.

formation to track the target. Compared with the traditional algorithm, the proposed algorithm has higher accuracy in maintaining formation flight to track the target, which also verifies its effectiveness and accuracy.

Figure 7 gives the error curve between the geometric centre trajectory and the target trajectory under different control algorithm. From the comparison results, it can be seen that the control error of the proposed algorithm is the smallest, which shows the feasibility and advantages of the proposed algorithm.

4. Conclusions

In this paper, we propose a robust control algorithm of coordinated formation tracking for multi-UAVs based on an artificial potential function. The convergence of the proposed artificial potential function is proved. A sliding mode control method with the saturation function is established, and its sufficient condition for reaching the sliding manifold is analysed. The simulation results show that after a short period, the proposed algorithm enables the tracking UAV to accurately track a target in a formation, which has a higher tracking accuracy and reduces the rotation buffeting of UAVs under a certain degree. The research results can provide a theoretical basis for engineering practice in the fields of dynamic target obstacle avoidance and swarm intelligent control.

Data Availability

The data used to support the findings of this study are included within the article.

Conflicts of Interest

The authors declare that they have no conflicts of interest.

Acknowledgments

This work is supported by the National Natural Science Foundation of China (61973094), the Maoming Natural Science Foundation (2020S004), and the Guangdong Basic and Applied Basic Research Fund Project (2020B1515310003).

References

[1] H. J. Zhao, J. Wang, Y. Q. Chen, and S. Ju, "Iterative learning-based formation control for multiple quadrotor unmanned

aerial vehicles," *International Journal of Advanced Robotic Systems*, vol. 17, no. 2, p. 172988142091152, 2020.

[2] S. L. Liao, R. M. Zhu, N. Q. Wu, T. A. Shaikh, M. Sharaf, and A. M. Mostafa, "Path planning for moving target tracking by fixed-wing UAV," *Defence Technology*, vol. 16, no. 4, pp. 811–824, 2020.

[3] W. H. Zhang, X. L. Shao, W. D. Zhang, J. P. Qi, and H. Z. Li, "Unknown input observer-based appointed-time funnel control for quadrotors," *Aerospace Science and Technology*, vol. 126, article 107351, 2022.

[4] A. Mahmood and Y. Kim, "Leader-following formation control of quadcopters with heading synchronization," *Aerospace Science and Technology*, vol. 47, pp. 68–74, 2015.

[5] R. Rakkiyappan, B. Kaviarasan, and J. H. Park, "Leader-following consensus for networked multi-teleoperator systems via stochastic sampled-data control," *Neurocomputing*, vol. 164, pp. 272–280, 2015.

[6] X. L. Shao, Y. Shi, and W. D. Zhang, "Input-and-Measurement Event-Triggered Output Feedback Chattering Reduction Control for MEMS Gyroscopes," *IEEE Transactions on Systems Man Cybernetics-Systems*, 2021.

[7] F. H. He, Y. Wang, Y. Yao, L. Wang, and W. S. Chen, "Distributed formation control of mobile autonomous agents using relative position measurements," *IET Control Theory and Applications*, vol. 7, no. 11, pp. 1540–1552, 2013.

[8] J. P. Desai, J. P. Ostrowski, and V. Kumar, "Modeling and control of formations of nonholonomic mobile robots," *IEEE Transactions on Robotics and Automation*, vol. 17, no. 6, pp. 905–908, 2001.

[9] M. A. Lewis and K. Tan, "High precision formation control of mobile robots using virtual structures," *Autonomous Robots*, vol. 4, no. 4, pp. 387–403, 1997.

[10] T. Balch and R. C. Arkin, "Behavior based formation control for multi-robot teams," *IEEE Transactions on Robotics and Automation*, vol. 14, no. 6, pp. 926–939, 1998.

[11] J. Wang, X. Nian, and H. Wang, "Consensus and formation control of discrete time multi-agent systems," *Journal of Central South University of Technology*, vol. 18, no. 4, pp. 1161–1168, 2011.

[12] X. W. Dong, Y. Zhou, and R. Zhang, "Time-varying formation tracking for second-order multi-agent systems subjected to switching topologies with application to quadrotor formation flying," *IEEE Transactions on Industrial Electronics*, vol. 64, no. 6, pp. 5014–5024, 2017.

[13] Y. Kuriki and T. Namerikawa, "Formation control with collision avoidance for a multi-UAV system using decentralized MPC and consensus-based control," *Journal of Control, Measurement, and System Integration*, vol. 8, no. 4, pp. 285–294, 2015.

[14] O. Saif, I. Fantoni, and A. Zavalario, "Distributed integral control of multiple UAVs: precise flocking and navigation," *IET Control Theory and Applications*, vol. 13, no. 13, pp. 2008–2017, 2019.

[15] M. Tomimasu, K. Morihiro, H. Nishimura, and N. A. Matsui, *Reinforcement Learning Scheme of Adaptive Flocking Behavior, International Conference on Knowledge-Based and Intelligent Information and Engineering Systems*, Google Scholar, Oita, Japan, 2006.

[16] K. Morihiro, T. Isokawa, H. Nishimura, and N. Matsui, "Characteristics of flocking behavior model by reinforcement learning scheme," in *SICE-ICASE international joint conference, Busan, South Korea*, pp. 4551–4556, IEEE, 2006.

[17] H. M. La and W. Sheng, "Distributed sensor fusion for scalar field mapping using mobile sensor networks," *IEEE Transactions on Cybernetics*, vol. 43, no. 2, pp. 766–778, 2013.

[18] H. M. La, R. Lim, and W. Sheng, "Multirobot cooperative learning for predator avoidance," *IEEE Transactions on Control Systems Technology*, vol. 23, no. 1, pp. 52–63, 2015.

[19] C. Wang, J. Wang, and X. Zhang, "A deep reinforcement learning approach to flocking and navigation of UAVs in large-scale complex environments," in *IEEE Global Conference on Signal and Information Processing (GlobalSIP)*, pp. 1228–1232, Anaheim, USA, 2018.

[20] H. Oh, S. Kim, H. S. Shin, A. Tsourdos, and B. White, "Coordinated standoff tracking of groups of moving targets Using multiple UAVs," in *21st Mediterranean Conference on Control and Automation*, pp. 967–977, Platanias, Greece, 2013.

[21] R. T. Ji, X. Z. Zhou, H. P. Wang, and Z. Q. Song, "Standoff tracking research based on Lyapunov method and potential field method," *Fire Control & Command Control*, vol. 41, no. 4, pp. 66–69, 2016.

[22] H. D. Chen, K. Chang, and C. S. Agate, "UAV path planning with tangent plus-Lyapunov vector field guidance and obstacle avoidance," *IEEE Transactions on Aerospace and Electronic Systems*, vol. 49, no. 2, pp. 840–856, 2013.

[23] J. Luo, "Cooperative tracking of a ground target with UAVs using Lyapunov guidance vector field," *Journal of Fudan University (Natural Science)*, vol. 51, no. 4, pp. 406–414, 2012.

[24] S. Lim, Y. Kim, D. Lee, and H. Bang, "Standoff target tracking using a vector field for multiple unmanned aircrafts," *Journal of Intelligent and Robotic Systems*, vol. 69, no. 1-4, pp. 347–360, 2013.

[25] A. A. Pothen and A. Ratnoo, "Curvature-constrained Lyapunov vector field for standoff target tracking," *Journal of Guidance, Control, and Dynamics*, vol. 40, no. 10, pp. 2729–2736, 2017.

[26] J. Y. Yao, R. Ordonez, and V. Gazi, "Swarm tracking using artificial potentials and sliding mode control," in *Proceedings of the 45th IEEE Conference on Decision and Control*, pp. 749–754, San Diego, CA, USA, 2007.

[27] Y. Wang, X. Chen, D. Ran, Y. Zhao, Y. Chen, and Y. Bai, "Spacecraft formation reconfiguration with multi-obstacle avoidance under navigation and control uncertainties using adaptive artificial potential function method," *Astrodynamics*, vol. 4, no. 1, pp. 41–56, 2020.

[28] S. Renevey and D. A. Spencer, "Establishment and control of spacecraft formations using artificial potential functions," *Acta Astronautica*, vol. 162, pp. 314–326, 2019.

[29] H. H. Seo, H. Bang, and Y. J. Cheon, "Steering law of control moment gyros using artificial potential function approach," *Acta Astronautica*, vol. 157, pp. 374–389, 2019.

[30] X. L. Shao, J. T. Zhang, and W. D. Zhang, "Distributed Cooperative Surrounding Control for Mobile Robots with Uncertainties and Aperiodic Sampling," *IEEE Transactions on Intelligent Transportation Systems*, 2022.

[31] V. Gazi and K. M. Passion, *Swarm Stability and Optimization II*, Springer, Berlin Heidelberg, 2011.

[32] V. Gazi and R. Ordónez, "Target tracking using artificial potentials and sliding mode control," *International Journal of Control*, vol. 80, no. 10, pp. 1626–1635, 2007.

[33] I. Haskara, "On sliding mode observers via equivalent control approach," *International Journal of Control*, vol. 71, no. 6, pp. 1051–1067, 1998.